Electronic Supplementary Information for: Coacervation of poly-electrolytes in the presence of lipid bilayers: Mutual alteration of structure and morphology

Sayantan Mondal[†] and Qiang Cui[*,†,‡,¶]

†*Department of Chemistry, Boston University, 590 Commonwealth Avenue, Boston, MA 02215, United States*

‡*Department of Physics, Boston University, 590 Commonwealth Avenue, Boston, MA 02215, United States*

¶*Department of Biomedical Engineering, Boston University, 44 Cummington Mall, Boston, MA 02215, United States*

E-mail: qiangcui@bu.edu, Tel:(+1)-617-353-6189

I. Contact pair analysis

In Figure 1 of the main text, we show the change in the number of self-contacts between polyelectrolytes (Q_{PP}); and cross-contacts between polyelectrolyte-lipid (Q_{PL}) and polyelectrolyte-ions (Q_{P-Ion}). Here we provide microscopic details by further decomposing the number of contacts into sub-components in Figure S1.

From Figure S1, it is clear that a large fraction of polyelectrolyte-lipid contacts is formed due to increased interaction between poly-K and POPG. On the other hand, the number of contacts decreases between K-K and E-K pairs. For E-E pairs, the number of contacts

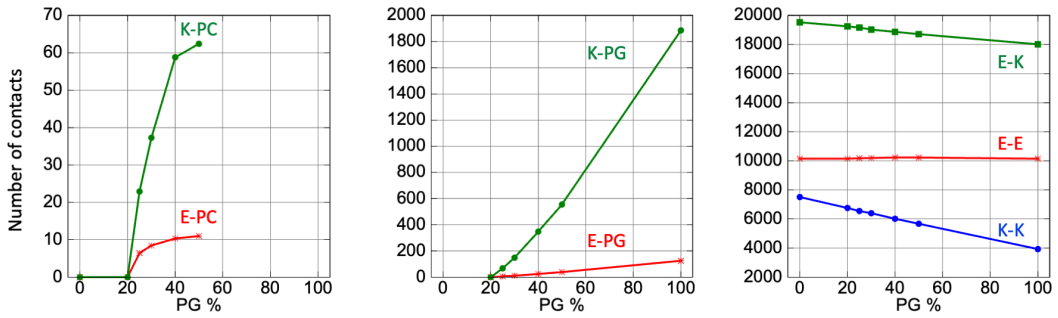

Figure S1: Number of contacts between different polyelectrolyte-lipid pairs in terms of different components.

slightly increases from 0 to 50 and then decreases again for the pure POPG system due to complete wetting. However, the magnitude of this change is overshadowed by the changes in the other two pairs, namely K-K and E-K.

II. Single chain end-to-end distributions

The single-chain properties are shown to influence the phase behavior of disordered peptides. We studied the end-to-end distance distribution of single chains in solution, in the coacervate phase, and in the membrane adsorbed state. The results are shown in Figure S2. We find that the distribution of the single-chain is different from chains in the coacervate/adsorbed phases. However, the end-to-end distributions are weakly dependent on the lipid bilayer composition and the extent of wetting.

III. Component wise energetics

In Figure 5 of the main text, we show the interaction energies of the coacervate with other components. Here we further decompose the interaction energies into several sub-components and show them in Figure S3.

We find that a large fraction of the gain in the polyelectrolyte-lipid interaction energy arises due to the favorable interactions between poly-K and POPG. On the other hand, the depleting E-K interactions can be identified as a major source of the destabilizing effect. As

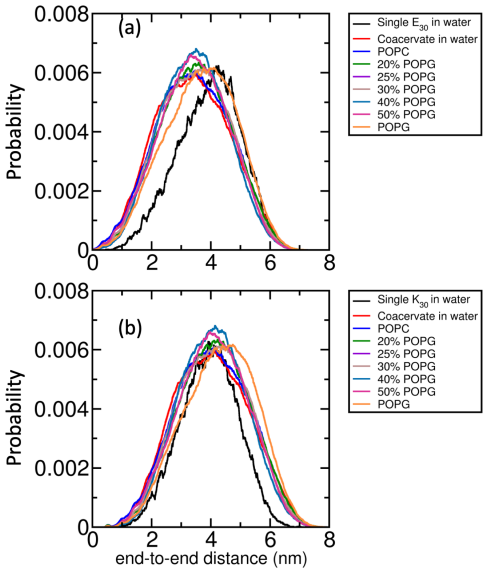

Figure S2: End-to-end distributions for (a) E_{30} and (b) K_{30} polyelectrolytes.

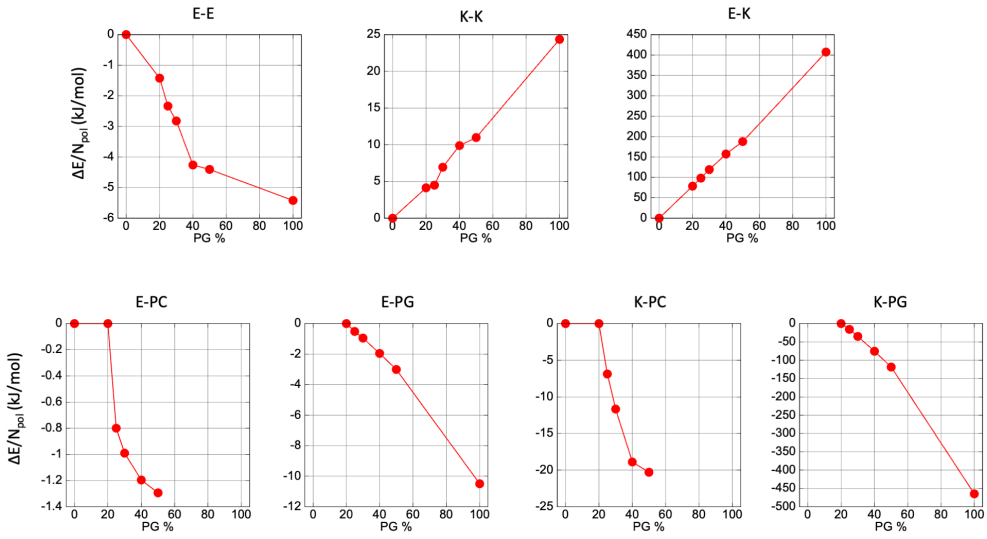

Figure S3: Component wise interaction energies of different polyelectrolyte-lipid pairs against lipid composition.

mentioned in the main text, we see that E-E interactions are somewhat stabilizing although its magnitude is again overshadowed by other interacting pairs.

IV. Curvature estimation from geometric fits

In order to find out the numerical values of the curvature, we use the time-averaged Z-surfaces, shown in Figure 3 of the main text, and fit the central region [approximately $10\ nm < X < 20\ nm$ and $10\ nm < Y < 20\ nm$] to a sphere. The obtained radii (R) are converted into the corresponding curvatures ($= 1/R$) and are tabulated in Table S1.

Table S1: Numerical values of the membrane negative curvature obtained from three-dimensional spherical fits.

	Curvature in nm^{-1}	
% POPG	No excess ion	0.15M $NaCl$
30	0.103	-
40	0.187	0.086
50	0.198	0.096

V. Effect of excess salt concentration

We carry out two kinds of analysis by increasing the salt concentration of the medium. (a) By adding 0.15M excess NaCl, where we find that the coacervate remains intact and wets the bilayer. Hence, we calculated several properties and find that the basic features of coacervate-lipid interactions remain unchanged. (b) By increasing the ionic strength to 0.4M and beyond to check whether the membrane could facilitate the coacervate formation as it is not observed in the solution phase studies.

a. Comparison of interaction energetics and number of contacts

In the main text (Figure 8), we show the effect of 0.15M excess NaCl on various properties of the coacervate and membrane. Here we provide the numerical values of the interaction energies that are represented as a bar plot in Figure 8(a) and component-wise contact pairs. There we subtracted the energies from the corresponding values in the pure POPC system (used as a control). Here we provide the absolute values of energy in Table S2 and the number of contacts for different pairs in Table S3.

Table S2: Comparison of the interaction energies with and without the presence of excess ions. The averages and errors are calculated from block averages where each block of data consists of 500 ns trajectory.

	Average energy per polyelectrolyte (kJ/mol)		
% POPG	Pairs	No excess ion	0.15M $NaCl$
40	P-P	-1357.4 ±5.9	-1132.9 ± 5.2
	P-L	-97.5 ±4.2	-44.1 ± 7.3
	P-Ion	-195.8 ±4.3	-539.00 ± 6.5
50	P-P	-1325.8 ±3.4	-1116.2 ± 4.4
	P-L	-142.9 ±7.9	-70.4 ± 6.4
	P-Ion	-233.1 ±3.9	-550.7 ± 4.2

Table S3: Comparison of the component wise time averaged number of contacts with and without the presence of excess ions. The averages and errors are calculated from block averages where each block of data consists of 500 ns trajectory.

% POPG	Pairs	No excess ion	0.15M $NaCl$
40	E-E	10230.3 ±17.5	10177.41 ±12.2
	K-K	18866.5 ±38.7	18219.9 ±29.4
	E-K	6008.0 ±28.2	3910.4 ±50.5
	E-PC	10.9 ±0.7	4.0 ±0.6
	E-PG	24.7 ±0.9	7.9 ±1.5
	K-PC	58.8 ±2.5	25.0 ±4.8
	K-PG	347.57 ±15.9	157.5 ±26.0
	E-Ion	1104.2 ±28.4	2376.0 ±30.9
	K-Ion	367.2 ±9.9	1805.7 ±43.1
50	E-E	10222.7 ±16.1	10185.6 ±16.4
	K-K	18714.5 ±44.8	18170.5 ±32.4
	E-K	5676.5 ±66.5	3767.6 ±41.6
	E-PC	10.4 ±0.7	4.9 ±0.9
	E-PG	38.9 ±2.8	14.1 ±1.7
	K-PC	62.4 ±3.5	35.7 ±3.7
	K-PG	554.6 ±38.1	302.4 ±26.7
	E-Ion	1320.4 ±21.7	2459.1 ±23.6
	K-Ion	416.7 ±20.1	1795.3 ±39.2

b. Effect of higher ionic strengths

In the earlier experimental and theoretical studies on E_{30}-K_{30} mixtures in the bulk phase, coacervation was not observed beyond 0.4M NaCl concentration. We simulate the same systems, but in the presence of a lipid bilayer, to see whether membranes can facilitate coacervation at 0.4M and 0.6M NaCl concentrations. From 3 μs trajectories, we observe

that the coacervate gets dissolved and a significant fraction of polyelectrolytes get desorbed from the membrane surface [Figure S4].

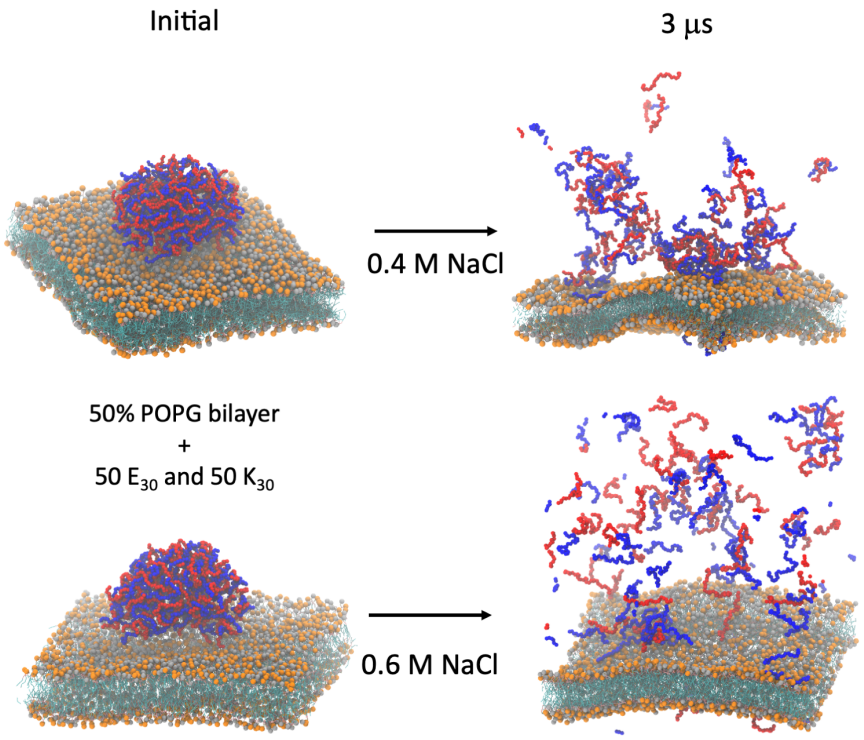

Figure S4: Effect of excess salt-concentration, namely 0.4M and 0.6M, on the wetting of the membrane by the polyelectrolyte coacervate. For both the concentrations the coacervate gets dissolved and a significant number of polyelectrolytes gets desorbed from the lipid bilayer.

VI. Comparison with atomistic simulations

In order to test the robustness of the analyses based on interaction energetics with Martini 3.0, we perform the following two types of analyses: (a) We first test whether the enthalpy-entropy balance is preserved for polyelectrolyte association and (b) whether the relative increase/decrease in the interaction energies are correctly predicted by Martini 3 parameters.

a. Driving force of polyelectrolyte association

Earlier studies reveal that polyelectrolyte association (at room temperature) is an entropy driven process [Ref. 44 in the main text]. This was tested by decomposing the potential of

mean force (PMF) into enthalpic and entropic components, using atomistic (AMBERff99sb) and coarse-grained (POL-Martini and BMW-Martini) force-fields. Here we perform the same analysis by using Martini 3 force-field. We calculate the PMFs (ΔA) against the distance ($\xi_{Glu-Lys}$) between E_{11} and K_{11} polyelectrolytes, by employing umbrella sampling simulations at two different temperatures, namely T_1=280 K and T_2=320 K [Figure S5(a)] in an NVT ensemble, as was done in the aforementioned study. Then we used Eq. (S1) to decompose the PMF into entropic ($-T\Delta S$) and enthalpic (ΔU) contributions [Figure S5(b)]. We observe that, Martini 3 captures the balance between entropy and enthalpy relatively well, in the context of polyelectrolyte association.

$$\Delta S(\xi) = -\frac{\Delta A(\xi, T_2) - \Delta A(\xi, T_1)}{T_2 - T_1}$$
$$\Delta U(\xi) = \Delta A(\xi) + T\Delta S(\xi) \tag{S1}$$

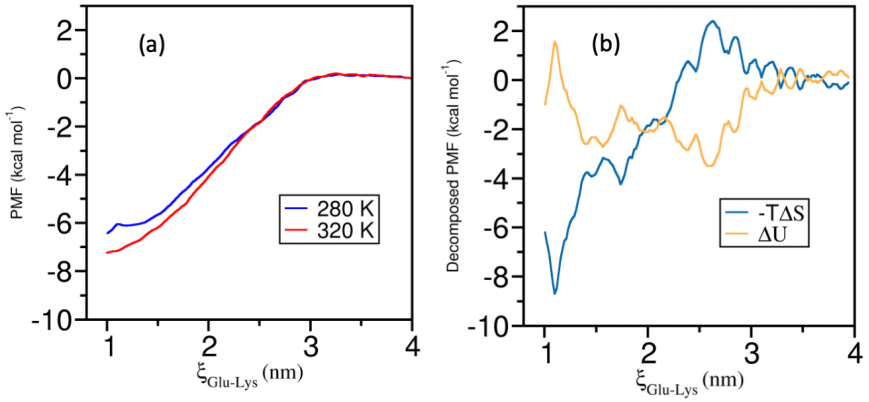

Figure S5: (a) PMFs as a function of distance between E_{11} and K_{11} polyelectrolytes, at two different temperatures. (b) Decomposition of the PMF at 320 K into entropic and enthalpic components. As in previous work [Ref. 44 in the main text], the simulations are conducted with finite counter ion concentration; in particular, each polyelectrolyte chain has been individually neutralized with counter ions (Na^+, Cl^-).

b. Energetics of coacervate-membrane interaction

Here we compare the energetics of membrane adsorption by constructing two (12 nm × 12 nm × 18 nm) systems, one with CHARMM36m (with TIP3P) atomistic forcefield and another with Martini-3. These systems contain 10 molecules of each E_{11} and K_{11} with a 12 nm × 12 nm patch of the lipid bilayer (composition PC:PG=50:50) spanning in the XY-direction. In

addition to that, we simulate the same number of polyelectrolytes in a $(12\ nm)^3$ cubic box that works as the respective reference points. Some representative snapshots are provided in Figure S6. The comparison of energetics is given in Table S4.

Table S4: Comparison of energy components per polyelectrolyte, between CHARMM36m atomistic simulations and MARTINI-3 CG simulations. The respective bulk simulations are used as reference. $\Delta E =< E > - < E >_{bulk}$.

	$\Delta E/N_{pol}$ (kJ/mol)	
Components	CHARMM36m	MARTINI-3
P-P	21.2 ± 10.3	109.2 ± 4.0
P-L	-102.5 ± 10.8	-138.6 ± 5.2
P-Ion	-11.1 ± 2.5	-137.9 ± 3.1

It is interesting to note that Martini-3 simulations, despite the absence of long-range electrostatics, capture the same qualitative trend as the atomistic simulations. That is, upon membrane adsorption the polyelectrolyte-polyelectrolyte (P-P) interaction decreases and gets compensated by the increase in the polyelectrolyte-lipid (P-L) and polyelectrolyte-ion (P-Ion) interactions. The relative magnitudes indeed differ, which is likely due to the relatively short (100 ns) atomistic trajectory that leads to limited sampling and an incomplete ion permeation into the coacervate. Additionally, we observe a small negative curvature being induced around the region of adsorption, even in the atomistic simulation.

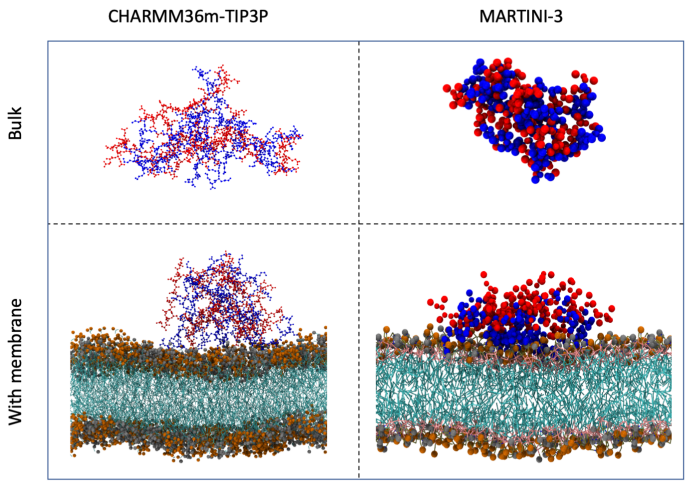

Figure S6: Snapshots from atomistic (left panel) and Martini 3 (right panel) simulations after 100 ns and 1 μs of production run, respectively.